

CANCER

Lymph node metastases can invade local blood vessels, exit the node, and colonize distant organs in mice

Ethel R. Pereira,¹ Dmitriy Kedrin,^{1,2} Giorgio Seano,¹ Olivia Gautier,^{1,3} Eelco F. J. Meijer,¹ Dennis Jones,¹ Shan-Min Chin,¹ Shuji Kitahara,¹ Echoe M. Bouta,¹ Jonathan Chang,^{4,5} Elizabeth Beech,¹ Han-Sin Jeong,⁶ Michael C. Carroll,^{5,7} Alphonse G. Taghian,⁸ Timothy P. Padera^{1*}

Lymph node metastases in cancer patients are associated with tumor aggressiveness, poorer prognoses, and the recommendation for systemic therapy. Whether cancer cells in lymph nodes can seed distant metastases has been a subject of considerable debate. We studied mice implanted with cancer cells (mammary carcinoma, squamous cell carcinoma, or melanoma) expressing the photoconvertible protein Dendra2. This technology allowed us to selectively photoconvert metastatic cells in the lymph node and trace their fate. We found that a fraction of these cells invaded lymph node blood vessels, entered the blood circulation, and colonized the lung. Thus, in mouse models, lymph node metastases can be a source of cancer cells for distant metastases. Whether this mode of dissemination occurs in cancer patients remains to be determined.

Solid tumor progression is characterized by metastasis to regional lymph nodes and dissemination to distant organs. The presence of lymph node disease in cancer patients correlates with a poorer prognosis and partially dictates the course of treatment (1–5). However, there is a robust ongoing debate about the role of lymph node metastasis in further progression of disease (6, 7). Some experts contend that localized lymph node metastases are clinically inconsequential (8, 9), whereas others contend that lymph node metastases have the potential to seed distant organs (5, 10–12) and therefore should be treated to prevent distant metastasis (13, 14). This debate has taken on new urgency with the recent completion of clinical trials that suggest that nodal dissection beyond the sentinel (first) lymph node does not provide therapeutic benefit to patients who have received adjuvant radiation therapy and systemic therapies (15–19). Other data show that radiation therapy of regional lymph nodes improves the outcome of patients with early stage breast cancer (20, 21), suggesting that treatment of metastatic lymph nodes benefits a subgroup of patients (22, 23).

In this study, we used mouse models to investigate whether cancer cells can exit the lymph node and disseminate to distant sites. We stably expressed the photoconvertible fluorescent protein Dendra2 (cytosolic localization) or Dendra2 fused to the nuclear protein histone H2B (Dendra2H2B nuclear localization) in 4T1 murine mammary cancer cells (a model of triple-negative breast cancer), B16F10 murine melanoma cells, and SCCVII murine squamous cell carcinoma cells. Dendra2 is a green-emitting fluorescent protein that can be converted to emit red light by exposure to 405-nm light (24). Expression of Dendra2 in these cell lines did not affect cell migration, proliferation rates, or in vivo tumor growth when compared with parental lines (fig. S1). We orthotopically implanted tumor cells into syngeneic mice and resected the primary tumor once it reached a volume of ~250 to 500 mm³. Next, we used a 405-nm laser diode on 5 consecutive days to convert Dendra2H2B cancer cells from green to red fluorescence, restricting the light exposure to the metastatic lymph node (Fig. 1A). Tissue clearing of the resected primary tumor revealed that no cancer cells at the primary site underwent spontaneous photoconversion (fig. S2). The in vivo photoconversion efficiency in the lymph node was 70% for 4T1 cells, 62% for B16F10 cells, and 56% for SCCVII cells (fig. S3).

We next determined whether photoconverted circulating tumor cells (CTCs) appeared in the blood of animals that had undergone photoconversion of the lymph node. The presence of red fluorescent CTCs would show that these cells originated from lymph node metastases. We identified red photoconverted 4T1 CTCs and B16F10 CTCs (Fig. 1, B and C, and fig. S4, A and B) that disseminated from the lymph node. CTCs from 4T1-Dendra2 and 4T1-Dendra2H2B lymph node

metastasis were grown in vitro to confirm viability. Both viable red (lymph node origin) and green fluorescent CTCs were observed after 1 day in culture. By day 7, only green colonies formed, as red fluorescence is lost as the photoconverted cells divide (fig. S4C). These data show that viable cancer cells from the lymph node have the potential to exit the node and survive in the blood. We did not detect photoconverted SCCVII CTCs (Fig. 1B and fig. S4D), although our methods could detect these cancer cells when photoconverted in vitro (fig. S5A) and in the lymph node of SCCVII tumor-bearing animals (fig. S5B).

To explore whether cancer cells in lymph nodes can seed distant organs, we analyzed the lungs of mice after photoconversion of their lymph node metastasis. Confocal microscopy revealed the presence of isolated photoconverted (red) cancer cells in the lungs of animals with 4T1 (Fig. 2, A and B) and B16F10 cancers (Fig. 2, C and D). Among the isolated cancer cells detected in the lung, 70% of 4T1 cells and 68% B16F10 cells were of lymph node origin (Fig. 2, B and D). We performed a spectral scan from 426 to 661 nm with a 5-nm bandwidth (fig. S6), which showed distinct signals for DAPI (4',6-diamidino-2-phenylindole) (emission maximum: 450 nm), native Dendra2H2B (emission maximum: 507 nm), and photoconverted Dendra2H2B (emission maximum: 572 nm) (24) in lung sections, with no detectable signal at other wavelengths. These data demonstrate the specificity of our detection methods to identify lung metastasis of lymph node origin. We did not detect cancer cells in the lungs of SCCVII-bearing mice.

We next evaluated whether the primary tumor can also seed the lung directly without transiting the lymph node. By photoconverting 4T1-Dendra2H2B primary tumors only (fig. S7A), before their dissemination to the draining lymph node (fig. S7B), we detected photoconverted CTCs (fig. S7C) in whole blood from these animals, which could only have originated from the primary tumor. Next, we prophylactically excised the sentinel lymph nodes from BALB/c mice (fig. S8) before injecting 4T1-Dendra2H2B cancer cells into the mammary fat pad (MFP). Two weeks after primary tumor resection, we detected CTCs and lung metastases in the absence of lymph nodes. However, animals with intact lymph nodes had higher numbers of CTCs and lung metastases compared with animals with lymph nodes removed (fig. S8). Taken together, these data show that cancer cells from the primary site can directly enter the systemic circulation and seed the lung.

We then examined whether both routes of metastasis—transit via the lymph node or transit directly from the primary tumor—can contribute to distant metastatic lesions. To this end, we injected Dendra2-expressing (green fluorescent protein) 4T1 cancer cells directly in the axillary lymph node (fig. S9A). On the contralateral side, the lymph node was removed 1 week before injection of mCherry-expressing (red fluorescent protein) 4T1 cancer cells into the MFP (Fig. 2E and fig. S9B). Ten days after resecting both the tumor-bearing lymph node and the MFP tumor, we detected both red and green lung metastases

¹Edwin L. Steele Laboratories, Department of Radiation Oncology, Massachusetts General Hospital (MGH) Cancer Center, MGH and Harvard Medical School (HMS), Boston, MA 02114, USA. ²Division of Gastroenterology, MGH and HMS, Boston, MA 02114, USA. ³Department of Biological Engineering, Massachusetts Institute of Technology, Cambridge, MA 02142, USA. ⁴Graduate Program in Immunology, Division of Medical Sciences, HMS, Boston, MA 02115, USA. ⁵Program in Cellular and Molecular Medicine, Children's Hospital Boston and HMS, Boston, MA 02115, USA. ⁶Department of Otorhinolaryngology and Head and Neck Cancer Center, Samsung Medical Center, Sungkyunkwan University School of Medicine, Seoul, South Korea. ⁷Department of Pediatrics, Children's Hospital Boston and HMS, Boston, MA 02115 USA. ⁸Department of Radiation Oncology, MGH and HMS, Boston, MA 02114, USA. *Corresponding author. Email: tpadera@steele.mgh.harvard.edu

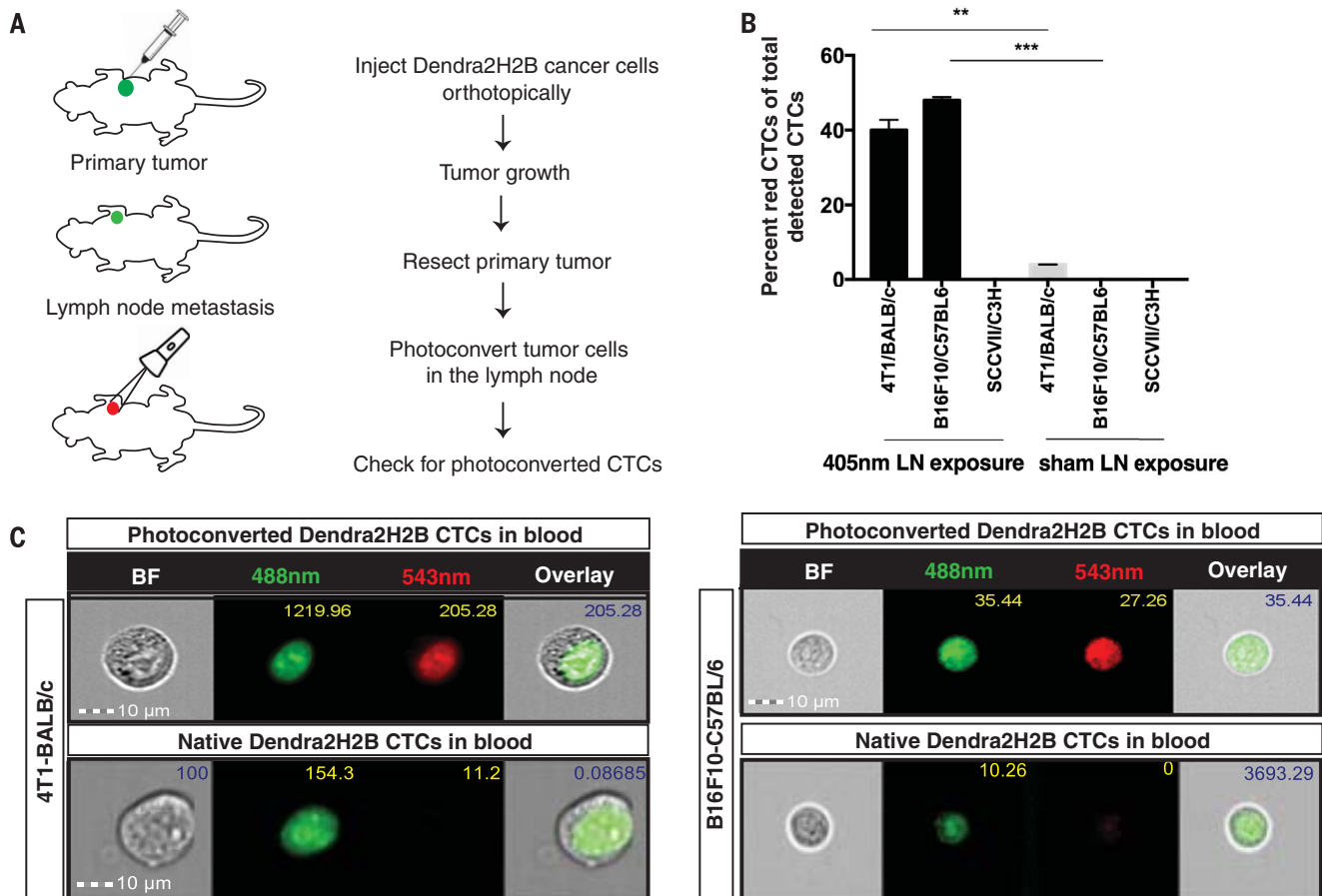


Fig. 1. Circulating tumor cells (CTCs) that transited through the lymph node are detected in mouse models. (A) Dendra2H2B-positive cancer cells were injected orthotopically into syngeneic recipients. Approximately 20 days later, the primary tumor was resected and tumor-draining lymph nodes were photoconverted using a 405-nm diode for 5 consecutive days. Blood was analyzed for the presence of green and red fluorescent CTCs using an Amnis ImageStream flow cytometer. (Photoconverted animals: 4T1 model, $n = 11$; B16F10 model, $n = 7$; SCCVII model, $n = 5$. Control animals: 4T1 model, $n = 5$; B16F10 model, $n = 7$; SCCVII, $n = 3$.) (B) Dendra2H2B-4T1 and Dendra2H2B-B16F10 cells but not

Dendra2H2B-SCCVII cells photoconverted in the draining lymph node (LN) were detected in the blood. Data are represented as the percentage of red CTCs (photoconverted) among total detected CTCs. Green CTCs were detected in all three models. For 405-nm light exposure compared with sham exposure for individual cell lines, $**P < 0.005$ and $***P < 0.0005$. Error bars indicate SEM. (C) Representative images obtained by ImageStream flow cytometry of CTCs from 4T1/BALB/c and B16F10/C57BL/6 mouse models show positive photoconverted cancer cells verified by nuclear localization of Dendra2H2B. Numbers indicate fluorescence intensity. BF, bright field.

(Fig. 2F; H&E staining in fig. S9C). We measured a large variation in the ratio of green:red metastatic lung lesions across multiple animals (average ratio of eight green:five red metastatic lesions) (Fig. 2G). Despite this large variation, every animal had lung metastases that originated from both lymph node lesions and directly from the primary tumor.

Cancer cells could take two possible routes to exit the lymph node and spread systemically—through lymph node blood vessels or efferent lymph. We hypothesized that cancer cells can escape the lymph node by directly invading lymph node blood vessels. Immunohistochemical analysis of 4T1 tumor-draining lymph nodes revealed isolated cancer cells (cytokeratin positive) in close association with CD31-positive blood vessels, within high endothelial venules and breaching the vascular basement membrane (collagen IV positive) (Fig. 3A). In metastatic lymph nodes with only isolated cancer cells (fig.

S10A), quantitative analysis showed that $23 \pm 2\%$ of isolated cancer cells were within $5 \mu\text{m}$ of a blood vessel, compared with only $11 \pm 1\%$ of cancer cells in a model of randomly distributed cells in the lymph node (Fig. 3, B and C, $P < 0.05$). Further, $6 \pm 2\%$ of the cancer cells were inside blood vessels (Fig. 3D and fig. S10B). A similar analysis performed in lymph nodes containing larger metastatic lesions ($>200 \mu\text{m}$ in diameter, fig. S11A) did not show this tropism (fig. S11B, $P > 0.05$). As metastatic lesions grow, the surface area of the blood vessels becomes limiting, causing the distribution of cancer cells to revert to that of a random distribution. This phenotype is consistent with the lack of sprouting angiogenesis in lymph node metastases (25). In lymph nodes with large lesions, $1 \pm 0.5\%$ of cancer cells were found in blood vessels (Fig. 3D). A similar analysis did not show an association between cancer cells and lymphatic vessels in tumor-draining lymph nodes (fig. S12, $P > 0.05$).

We also analyzed lymph nodes with large metastatic lesions from 19 patients with head and neck cancer. Similar to large lesions in mouse lymph nodes, cancer cells in human lymph nodes did not demonstrate measurable tropism to blood vessels, owing to the limitation in vessel surface area. However, at the edge of the metastatic lesions, we found cancer cells that were closely associated with blood vessels (fig. S13). In addition, we detected isolated cancer cells inside blood vessels in 6 of the 19 patient samples (fig. S13), consistent with our preclinical data.

To confirm that metastatic cancer cells in a lymph node have an affinity for lymph node blood vessels, we used time-lapse multiphoton intravital microscopy to measure cancer cell migration in an optical lymph node window in mice (25). Dendra2-expressing metastatic cancer cells are first seen in the subcapsular sinus and later invade the cortex of the lymph node. There, they accumulate around rhodamine-dextran-labeled

blood vessels (Fig. 4, A to C, and fig. S14) or associate with lymph node conduits, which contain a fibrillar collagen core surrounded by fibroblastic reticular cells (FRCs) (Fig. 4D). Cancer cells can be observed in directed migration toward blood vessels as well as moving inside blood vessels (movies S1 to S3 and Fig. 4E). Time-lapse imaging of tumor-draining lymph nodes revealed that only a small fraction of cancer cells in the lesion are motile. Both 4T1 and SCCVII cells that were motile had an average speed of 7 $\mu\text{m}/\text{hour}$ (Fig. 4F), similar to the speed of resident lymph node stromal cells such as FRCs, follicular dendritic cells, macrophages, and resident dendritic cells (26). However, a greater fraction of 4T1 cells were motile compared with SCCVII cells (Fig. 4G). Consistent with our observations in tissue sections (Fig. 3F), cancer cells create persistent associations with blood vessels (Fig. 4, B and C) as well as conduits (Fig. 4D). The conduit system is an interconnected collagen network formed by FRCs that creates pathways for dendritic cells to navigate through the lymph node to interact with naïve lymphocytes near high endothelial venules (27). We speculate that, similar to dendritic cells, cancer cells use the conduit system to aid in their migration to lymph node blood vessels.

The Dendra2 system has limitations. First, the photoconversion of the green Dendra2 protein to red fluorescence can be detected for only 5 to 6 days before the cells appear green again. Second, the photoconversion efficiency of Dendra2H2B in the lymph node was ~60 to 70% in our tumor models. Thus, in mice that underwent photoconversion of metastatic cancer cells in the lymph node, green-Dendra2H2B-expressing cancer cells in the blood or lungs could have multiple sources, including the primary tumor directly, unconverted cancer cells in the lymph node, or photoconverted cancer cells in the lymph node that lost their red fluorescence with cell division. These limitations prevent us from accurately assessing what percentage of distant metastases originates from lymph node metastases.

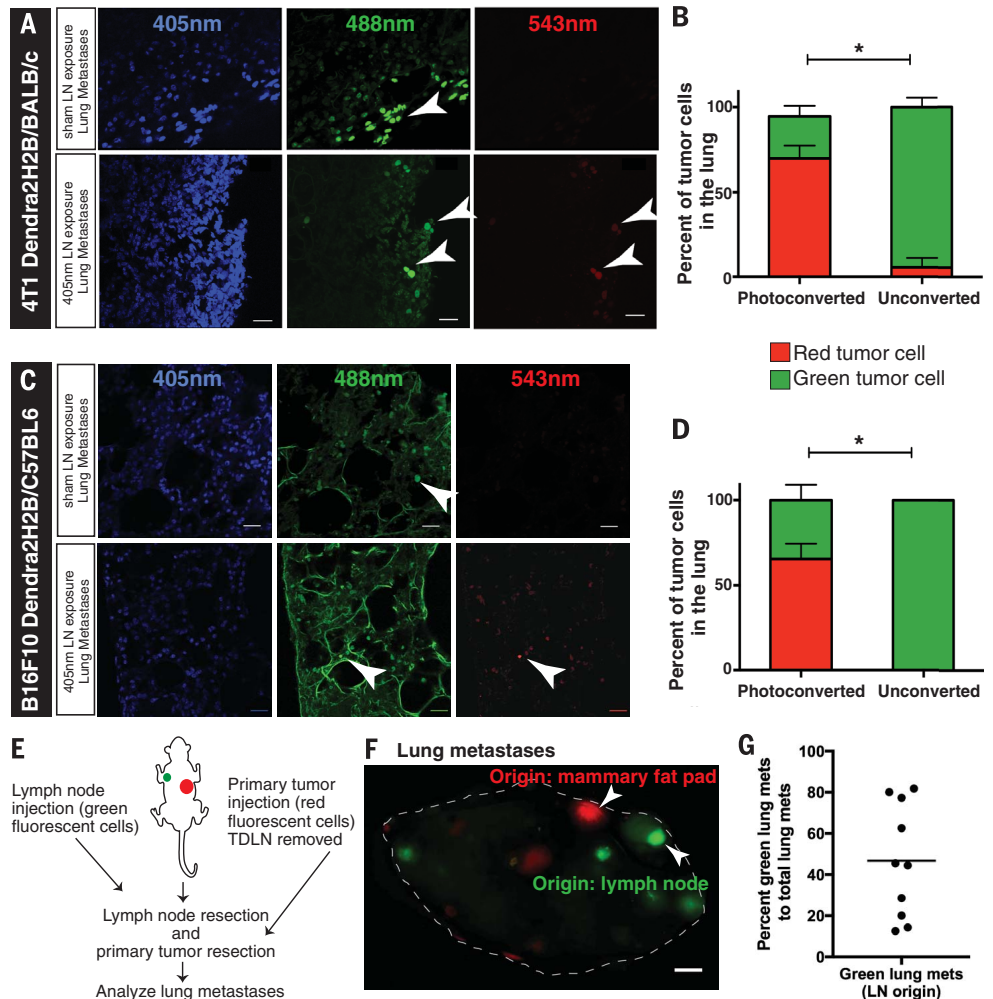
The absence of detectable photoconverted CTCs and lung metastasis in the SCCVII cancer model reflects the variability in the aggressiveness of cancer models in mice. We do not expect the selected mouse cell lines to represent the variability present in patient populations. Further, cancer cells alter their phenotype in response to local microenvironments as they spread to metastatic sites. We measured changes in the expression of chemokines—signaling molecules

that regulate cell homing and migration—as cancer cells spread from the primary tumor to the lymph nodes and lungs (fig. S15). These data may provide clues as to how cancer cells can navigate from one metastatic site to another.

The route of cancer cell dissemination to distant sites in patients is complex and highly debated, in part because of limited clinical and experimental evidence. However, animal studies have linked large lymph node metastases to distant metastases (28). Further, studies using patient lymph node samples, human mammary carcinoma cells, and xenograft tumors in immune-deficient mice have shown that cancer cells can invade lymphatic vessels in the sentinel lymph node and spread to additional nodes (29). Several clinical studies have also shown a relationship between the number of involved axillary lymph nodes and a higher risk for distant recurrence in breast cancer patients (13, 30, 31). Genetic studies examining the clonal relationships between cancer cells in the primary site, lymph nodes, and distant organs have shown that distant metastases are more closely related to lymph node metastases than to primary tumors in a subset of mice and patients (32, 33). Our mouse studies validate these data by directly showing

Fig. 2. Metastatic cancer cells in the lymph node can colonize the lung. (A and C) Sections (100- μm thickness) of fresh frozen lungs were obtained from Dendra2H2B-4T1 and Dendra2H2B-B16F10 tumor-bearing mice that either had their lymph nodes photoconverted with a 405-nm diode or had no photoconversion. The top panels are representative images of micrometastatic cancer cells (arrowheads) in the lung from control animals (no photoconversion), whereas the bottom panels show photoconverted isolated cancer cells that have colonized the lung via the lymph node.

Scale bars, 20 μm . (B and D) Percentage of cancer cells (green, not photoconverted; red, photoconverted) detected in the lungs of Dendra2H2B-4T1 ($n = 8$) and Dendra2H2B-B16F10 ($n = 8$) tumor-bearing mice. * $P < 0.05$ when we compared 405-nm light exposure (photoconverted) to sham light exposure (unconverted) for individual cells lines. Error bars indicate SEM. (E) Schematic of experiment to determine whether cancer cells injected directly in the lymph node and in the mammary fat pad (MFP) can both form large metastases in the lungs. TDLN, tumor-draining lymph node. (F) Image of a lung with red lesions (originating from the MFP) and green lesions (originating from the lymph node) marked by arrowheads. Scale bar, 1 mm. (G) Lung metastases are represented as the percentage of metastatic lesions (mets) of lymph node origin (green) among total macroscopic lesions (red and green) ($n = 10$ animals). As assessed by a one-sample Student's t test, metastatic lung lesions were shown to have originated from both lymph node and MFP tumors ($P < 0.001$).



Downloaded from https://www.science.org at University of Pennsylvania on June 10, 2022

Fig. 3. Cancer cells in the lymph node associate with blood vessels and invade the vascular basement membrane. (A) (i and iv) Immunofluorescence staining of metastatic lymph nodes with isolated 4T1 cancer cells (anti-cytokeratin, green), blood vessels (anti-CD31, red), and basement membrane (anti-collagen IV, blue) shows cancer cells associating with blood vessels (ii and v, arrowheads) and the vascular basement membrane (iii and vi, arrowheads). A cancer cell is observed inside a blood vessel (ii and iii) (arrowhead). Scale bars, 50 μm (i); 20 μm (iv); 10 μm (ii, iii, v, and vi). (ii) and (iii) represent zoomed-in views of the boxed area in (i); (v) and (vi) represent zoomed-in views of the boxed area in (iv). (B) Quantification of the fraction of cancer cells within 5 μm of a blood vessel (sample) in a lymph node compared with a theoretical random distribution (reference) of the same number of cells in the same lymph node shows cancer cell association with lymph node blood vessels. $n = 11$ individual lymph nodes $*P < 0.05$. (C) Representative histogram of the fraction of cancer cells at varying distances from the nearest blood vessel in a given lymph node with isolated cancer cells (sample) compared with the reference distribution for that lymph node (reference). The measured distribution shows an association of cancer cells with blood vessels in the lymph node. (D) Quantification of the fraction of cancer cells inside a blood vessel in lymph nodes containing macro-metastatic lesions (lesions) or isolated tumor cells (ITC).

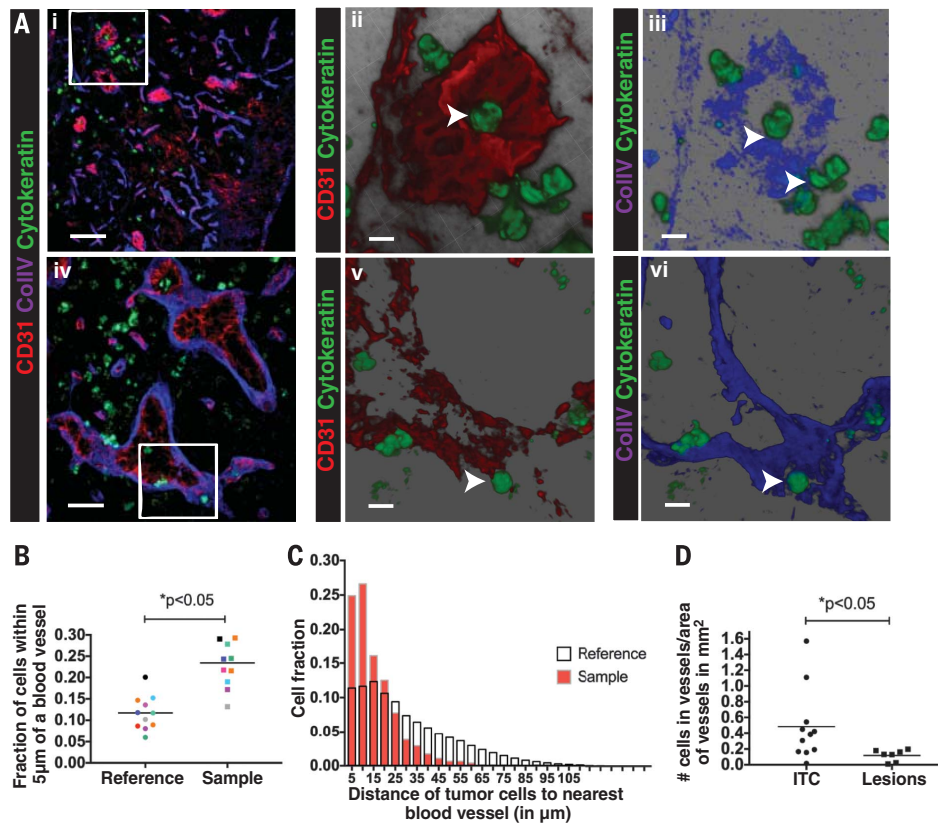
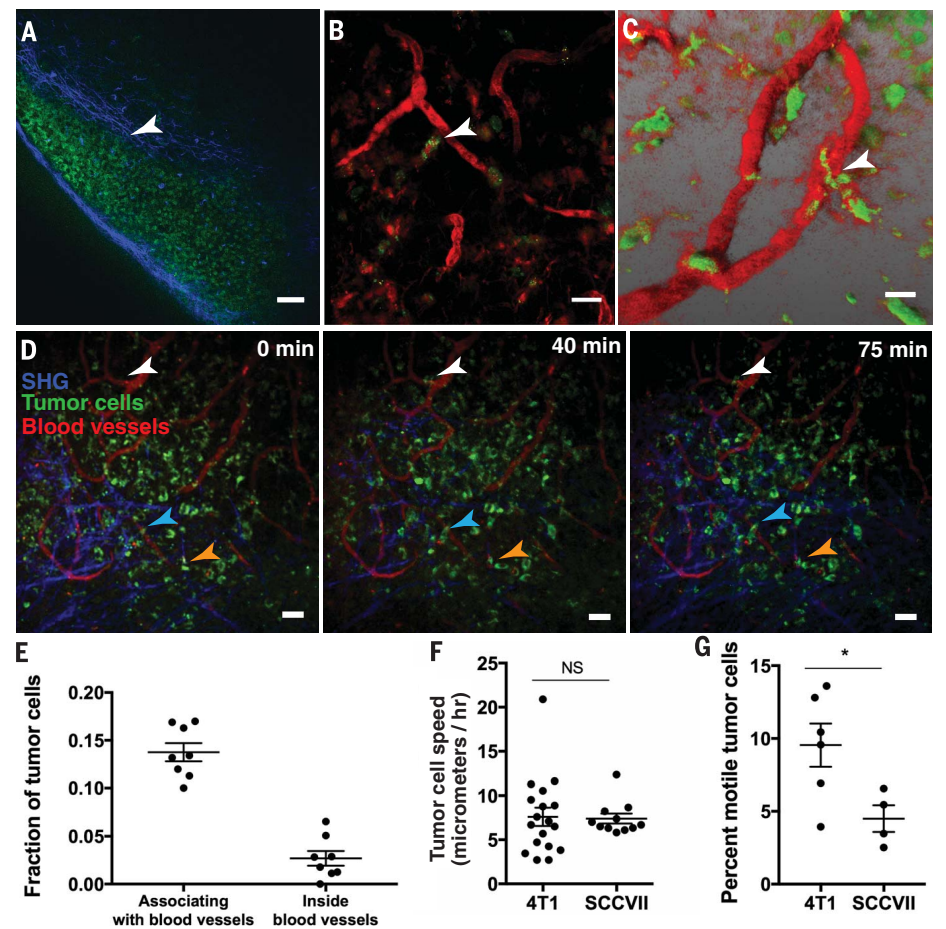


Fig. 4. Time-lapse intravital imaging of lymph node metastasis shows slow cancer cell migration toward blood vessels. (A) 4T1-Dendra2-expressing cancer cells (green fluorescence) form a large colony in the subcapsular sinus of the draining lymph node (arrowhead). Scale bar, 60 μm . (B and C) Cancer cells (green) that invaded the lymph node cortex wrapped around blood vessels (arrowheads), which were labeled by intravenous injection of rhodamine-dextran (red). Images were obtained by multiphoton microscopy at a depth of 80 to 110 μm below the surface of the lymph node. Scale bars, 20 μm . (D) Time-lapse intravital imaging of cancer cells (green) in association with blood vessels (red) and collagen fibers [blue, detected by second harmonic generation (SHG)] over the course of 75 min shows slow movement (arrowheads) of some cancer cells toward blood vessels. Images were obtained every 2 min, with a 50- μm z-stack. Scale bar, 50 μm . See also supplementary movies. (E) Quantification of the fraction of 4T1 tumor cells per field that associate with blood vessels or were inside blood vessels, analyzed by intravital microscopy in a tumor-draining lymph node. (F) Quantification of the speed of individual cancer cells in 4T1 and SCCVII lymph node metastases. (G) Quantification of the percentage of motile tumor cells in the image field over 75 min in 4T1 and SCCVII lymph node metastases. Quantification for (E) to (G) was performed on four to six individual mice. NS, not significant; $*P < 0.05$.



Downloaded from <https://www.science.org> at University of Pennsylvania on June 10, 2022

that lymph node metastases can be a source of cancer cells for distant metastases. Our data are similar to results obtained independently by Brown *et al.*, using different methodologies in mouse models (34). Additionally, we have revealed that lymph node metastases can disseminate by invading lymph node blood vessels rather than by transiting through efferent lymphatic vessels. Further studies are needed to determine whether dissemination of cancer cells from lymph nodes is a feature of human cancer and, if so, whether it should be a factor in treatment decisions.

REFERENCES AND NOTES

- I. Jatoi, S. G. Hilsenbeck, G. M. Clark, C. K. Osborne, *J. Clin. Oncol.* **17**, 2334–2340 (1999).
- K. Kawada, M. M. Taketo, *Cancer Res.* **71**, 1214–1218 (2011).
- R. L. Ferris, M. T. Lotze, S. P. Leong, D. S. Hoon, D. L. Morton, *Clin. Exp. Metastasis* **29**, 729–736 (2012).
- M. A. Saksena, A. Saokar, M. G. Harisinghani, *Eur. J. Radiol.* **58**, 367–374 (2006).
- H. Starz, B.-R. Balda, K.-U. Krämer, H. Büchels, H. Wang, *Cancer* **91**, 2110–2121 (2001).
- S. D. Nathanson, R. Shah, K. Rosso, *Semin. Cell Dev. Biol.* **38**, 106–116 (2015).
- E. R. Pereira, D. Jones, K. Jung, T. P. Padera, *Semin. Cell Dev. Biol.* **38**, 98–105 (2015).
- B. Cady, *Ann. Surg. Oncol.* **14**, 1790–1800 (2007).
- B. Fisher *et al.*, *N. Engl. J. Med.* **347**, 567–575 (2002).
- W. S. Halsted, *Ann. Surg.* **46**, 1–19 (1907).
- N. Cascinelli, A. Morabito, M. Santinami, R. M. MacKie, F. Belli, *Lancet* **351**, 793–796 (1998).
- S. D. Nathanson, D. Kwon, A. Kapke, S. H. Alford, D. Chitale, *Ann. Surg. Oncol.* **16**, 3396–3405 (2009).
- Early Breast Cancer Trialists' Collaborative Group (EBCTCG), *Lancet* **366**, 2087–2106 (2005).
- D. L. Morton *et al.*, *N. Engl. J. Med.* **370**, 599–609 (2014).
- A. E. Giuliano *et al.*, *JAMA* **305**, 569–575 (2011).
- V. Galimberti *et al.*, *Lancet Oncol.* **14**, 297–305 (2013).
- M. Donker *et al.*, *Lancet Oncol.* **15**, 1303–1310 (2014).
- R. Jagsi *et al.*, *J. Clin. Oncol.* **32**, 3600–3606 (2014).
- M. B. Faries *et al.*, *N. Engl. J. Med.* **376**, 2211–2222 (2017).
- P. M. Poortmans *et al.*, *N. Engl. J. Med.* **373**, 317–327 (2015).
- T. J. Whelan *et al.*, *N. Engl. J. Med.* **373**, 307–316 (2015).
- B. H. Ly, N. P. Nguyen, V. Vinh-Hung, E. Rapiti, G. Vlastos, *Breast Cancer Res. Treat.* **119**, 537–545 (2010).
- R. S. Punglia, M. Morrow, E. P. Winer, J. R. Harris, *N. Engl. J. Med.* **356**, 2399–2405 (2007).
- N. G. Gurskaya *et al.*, *Nat. Biotechnol.* **24**, 461–465 (2006).
- H. S. Jeong *et al.*, *J. Natl. Cancer Inst.* **107**, djv155 (2015).
- J. V. Stein, S. F. Gonzalez, *J. Allergy Clin. Immunol.* **139**, 12–20 (2017).
- J. E. Chang, S. J. Turley, *Trends Immunol.* **36**, 30–39 (2015).
- G. Crile Jr., W. Isbister, S. D. Deodhar, *Cancer* **28**, 657 (1971).
- D. Kerjaschki *et al.*, *J. Clin. Invest.* **121**, 2000–2012 (2011).
- J. Ragaz *et al.*, *N. Engl. J. Med.* **337**, 956–962 (1997).
- M. Overgaard *et al.*, *N. Engl. J. Med.* **337**, 949–955 (1997).
- D. G. McFadden *et al.*, *Cell* **156**, 1298–1311 (2014).
- K. Naxerova *et al.*, *Science* **357**, 55–60 (2017).
- M. Brown *et al.*, *Science* **359**, 1408–1411 (2018).

ACKNOWLEDGMENTS

We thank R. K. Jain for critical discussion, S. Mordecai for assistance with imaging experiments, and K. Piatkevich for assistance with laser diodes. **Funding:** This work was supported by NIH grants DP2OD008780, R01CA214913, and R01HL128168 (T.P.P.); National Cancer Institute

(NCI) Federal Share/MGH Proton Beam Income-C06CA059267 (T.P.P.); MGH Executive Committee on Research Interim Support Funding (T.P.P.); NIH grant T32 DK007191 (D.K.); Susan G. Komen Foundation Fellowship PDF14301739 (G.S.); a United Negro College Fund–Merck Science Initiative Postdoctoral Fellowship (D.J.); a Burroughs Wellcome Postdoctoral Enrichment Program Award (D.J.); NIH NCI grant F32CA183465 (D.J.); Korean Ministry of Education, Science, and Technology grant NRF-2012RIA1A2040866 (H.-S.J.); Samsung Biomedical Research Institute grant GLIB22912 (H.-S.J.); and NIH grant P01CA080124 (T.P.P.). We thank M. Vangel and Harvard Catalyst, the NIH (award UL1 TR001102), and Harvard University for assistance with biostatistical methods and financial contributions. **Author contributions:** E.R.P., D.K., and T.P.P. conceived and designed experiments. E.R.P., D.K., G.S., O.G., E.F.J.M., D.J., S.-M.C., S.K., E.M.B., and E.B. performed experiments. E.R.P., G.S., O.G., and T.P.P. analyzed data. E.R.P., D.K., G.S., D.J., J.C., H.-S.J., M.C.C., A.G.T., and T.P.P. discussed results and strategy. T.P.P. supervised the study. E.R.P. and T.P.P. wrote the manuscript, which was revised and approved by all authors. **Competing interests:** The authors declare no competing financial interests. **Data and materials availability:** All data are available in the main paper or the supplementary materials.

SUPPLEMENTARY MATERIALS

www.sciencemag.org/content/359/6382/1403/suppl/DC1
Materials and Methods
Figs. S1 to S15
References (35–39)
Movies S1 to S3

8 November 2016; resubmitted 14 April 2017
Resubmitted 5 October 2017
Accepted 24 January 2018
10.1126/science.aal3622

Lymph node metastases can invade local blood vessels, exit the node, and colonize distant organs in mice

Ethel R. PereiraDmitriy KedrinGiorgio SeanoOlivia GautierEelco F. J. MeijerDennis JonesShan-Min ChinShuji KitaharaEchoe M. BoutaJonathan ChangElizabeth BeechHan-Sin JeongMichael C. CarrollAlphonse G. TaghianTimothy P. Padera

Science, 359 (6382), • DOI: 10.1126/science.aal3622

An alternate route for metastatic cells

Metastatic tumor cells are thought to reach distant organs by traveling through the blood circulation or the lymphatic system. Two studies of mouse models now suggest a hybrid route for tumor cell dissemination. Pereira *et al.* and Brown *et al.* used distinct methodologies to monitor the fate of tumor cells in lymph nodes. They found that tumor cells could invade local blood vessels within a node, exit the node by entering the blood circulation, then go on to colonize the lung. Whether this dissemination route occurs in cancer patients is unknown; the answer could potentially change the way that affected lymph nodes are treated in cancer.

Science, this issue p. 1403, p. 1408

View the article online

<https://www.science.org/doi/10.1126/science.aal3622>

Permissions

<https://www.science.org/help/reprints-and-permissions>

Use of this article is subject to the [Terms of service](#)

Science (ISSN 1095-9203) is published by the American Association for the Advancement of Science, 1200 New York Avenue NW, Washington, DC 20005. The title *Science* is a registered trademark of AAAS.

Copyright © 2018 The Authors, some rights reserved; exclusive licensee American Association for the Advancement of Science. No claim to original U.S. Government Works